A&A, 699, A240 (2025)
https://doi.org/10.1051/0004-6361/202453368

Astronomy & Astrophysics

Time to Sparkler

Accurate ages of lensed globular clusters at $z = 1.4$ with JWST photometry

Elena Tomasetti[1,2,⋆], Michele Moresco[1,2], Carmela Lardo[1,2], Frédéric Courbin[4,5], Raul Jimenez[4,5], Licia Verde[4,5], Martin Millon[6,7], and Andrea Cimatti[1,3]

[1] Dipartimento di Fisica e Astronomia "Augusto Righi" –Università di Bologna, via Piero Gobetti 93/2, 40129 Bologna, Italy
[2] INAF - Osservatorio di Astrofisica e Scienza dello Spazio di Bologna, via Piero Gobetti 93/3, 40129 Bologna, Italy
[3] INAF - Osservatorio Astrofisico di Arcetri, Largo E. Fermi 5, 50125 Firenze, Italy
[4] ICC, University of Barcelona, Marti i Franques 1, 08028 Barcelona, Spain
[5] ICREA, Pg. Lluis Companys 23, Barcelona 08010, Spain
[6] Kavli Institute for Particle Astrophysics and Cosmology and Department of Physics, Stanford University, Stanford, CA 94305, USA
[7] Institute for Particle Physics and Astrophysics, ETH Zurich, Wolfgang-Pauli-Strasse 27, 8093 Zurich, Switzerland

Received 9 December 2024 / Accepted 21 May 2025

ABSTRACT

Determining reliable ages for old stellar objects at different redshifts offers a powerful means to constrain cosmology without relying on a specific cosmological model. This is known as the 'cosmic clocks' method. Globular clusters (GCs), long recognised as hosts of the Universe's oldest stars, have served as archetypical cosmic clocks. However, their age estimates have traditionally been confined to redshift $z = 0$, limiting their role to constraining the present-day age of the Universe $t(z = 0) = t_0$. Here, we explore how to measure reliable ages of GCs well beyond $z = 0$, leveraging their potential to extend cosmic clock measurements to earlier epochs. Specifically, we used six-band JWST/NIRCam high-precision photometry of candidate stellar clusters in the Sparkler galaxy, located at redshift $z = 1.378$ and strongly lensed by the galaxy cluster SMACS J0723.3-7327. By employing stellar population models within a Bayesian inference framework, we constrained the clusters' ages, star formation histories, metallicities, and dust attenuation. The five compact sources previously identified as GCs, based on their red spectral energy distributions being consistent with the colours of old stellar systems, yield a formation age of 1.9 ± 0.4 Gyr on average. This result implies a total age of the Universe that aligns well with the Λ cold dark matter model derived from Planck18 data, even though no cosmological prior was imposed on the age of these objects, which were allowed to span up to 15 Gyr. Recent space-based observations have uncovered a wealth of lensed GCs as well as globulars within the member galaxies of the clusters themselves. These findings suggest that the pool of objects available for cosmic clock studies is enormous. A systematic multi-band photometric survey of GCs in and behind galaxy clusters, using facilities like Euclid and the James Webb Space Telescope, would therefore be a powerful tool for estimating cluster ages across a large range of redshifts, allowing the Universe to be dated across an unprecedented range of epochs.

Key words. globular clusters: general – cosmological parameters – cosmology: observations

1. Introduction

Galactic globular clusters (GCs) are among the oldest stellar objects in our Galaxy and thus provide a valuable and fully cosmology-independent bound on the age of the Universe, which, in turn, can provide stringent constraints on cosmological models (e.g. Jimenez et al. 2019; Valcin et al. 2020; Cimatti & Moresco 2023). GCs are known to be single stellar populations (SSP) in age. While showing evidence for the presence of multiple stellar populations, these remain limited to the chemical composition, especially in light-element abundances[1] (e.g. Bastian & Lardo 2018; Gratton et al. 2019). Thus, the nuclear reactions inside the stars make GCs natural 'nuclear clocks'. The oldest GCs can then be used as cosmic clocks.

Traditionally, the ages of GCs have been computed from the colour-magnitude diagrams of their resolved stellar populations (e.g. VandenBerg et al. 2013; Gallart et al. 2005). This limits their use as cosmic clocks to $z = 0$.

To date, only passively evolving galaxies have provided cosmic clocks at higher redshifts (e.g. Moresco et al. 2012; Moresco 2015; Moresco et al. 2016; Ratsimbazafy et al. 2017; Borghi et al. 2022; Tomasetti et al. 2023; Jimenez et al. 2023), offering a cosmology-independent constraint on the expansion history of the Universe (Moresco et al. 2022). Recently, however, it has been shown that precise and accurate ages can be obtained from the integrated light of GCs (e.g. Koleva et al. 2008; Cezario et al. 2013; Gonçalves et al. 2020; Cabrera-Ziri & Conroy 2022; Tomasetti et al. 2025), which opens up the possibility of measuring the ages of extragalactic GCs at $z > 0$, as we demonstrate in this paper. Thus, in principle, GCs at high redshift can be cosmic (nuclear) clocks – complementary and independent from passively evolving galaxies – and yield a robust lower-limit on the age of the Universe at their observed redshift, provided that their age can be reliably measured.

The GCs are intrinsically faint, with absolute V-band magnitudes of $M_V = -7.5$ (Baumgardt et al. 2020). They are hardly visible at any redshift $z > 0.1$. At $z = 1$ they have apparent

⋆ Corresponding author: elena.tomasetti2@unibo.it

[1] A small subset of GCs, such as ω Cen, M 54, and Terzan 5, show significant spreads in iron-peak abundances among their stars. These clusters are among the most massive and make up only a few percent of the total GC population (e.g. Milone & Marino 2022).

magnitudes fainter than $V = 32$, clearly beyond the reach of any currently planned telescope. Fortunately, one can exploit gravitational lensing as a natural telescope that magnifies the apparent brightness of high-redshift GCs. As is the case for high redshift galaxies (Frontier Fields lensing clusters; Lotz et al. 2017), strong gravitational lensing magnifies the light of GCs, bringing them above the detection limits of current telescopes, particularly JWST.

Contrary to high-redshift galaxies, the angular extent of GCs is very small – a typical GC with an effective radius of 50 pc subtends a few milliarcsec at $z = 1-1.5$ – and their stellar population is very uniform across their light profile. This has the dual advantage that the magnifications can be very large and that there is no chromatic effect due to lensing in the spectral energy distribution (SED) of the GCs. Ages can therefore be measured in a clean way.

In addition, observing evolved GCs at z≫0.1 complements studies of local GCs (e.g. Tomasetti et al. 2025), with the further advantage that SEDs of younger stellar populations display an increased sensitivity to age (see e.g. Fig. 6 in Valcin et al. 2020). As a result, studying lensed GCs at redshifts $z \sim 1.5$ (corresponding to a third of the current age of the Universe in a vanilla ΛCDM cosmology) using JWST observations provides a promising solution.

In the present work, we use for the first time highly magnified GCs in a high-redshift ($z > 1$) galaxy as cosmic clocks. To do this, we consider the Sparkler galaxy, which is magnified by the $z = 0.39$ galaxy cluster SMACS J0723.3-7327 (Pontoppidan et al. 2022). The lensed source, with a magnification of 10–100, is a relatively low-mass galaxy at a redshift of $z = 1.38$ (Caminha et al. 2022; Mahler et al. 2023). Its total stellar mass is estimated as $\log(M_*/M_\odot) \approx 9.7$, which, after correcting for lensing, translates to an intrinsic mass between 5×10^8 and $1 \times 10^9\ M_\odot$ (Mowla et al. 2022; Claeyssens et al. 2023; Adamo et al. 2023, for more details). This galaxy has drawn significant attention as it displays prominent compact sources surrounding the main body of the galaxy itself. Most of these compact sources, referred to as 'the sparkles', remain unresolved even with JWST. Five of them have been identified as GC candidates (e.g. Mowla et al. 2022), owing to (1) the absence of [OIII] λ5007 emission, which is detected in the star-forming regions of the host galaxy but not at the locations of the GC candidates, and (2) their observed urJ colours, which again suggest that these systems were quiescent at the time of formation. Hereafter, we assume these candidates are indeed GCs.

Accurate and precise photometry of these objects is crucial to derive reliable ages from SED fitting. However, obtaining reliable photometry of faint point sources superposed on a complex light distribution that changes morphology between bands and in presence of a very complex point-spread function (PSF) is a challenging task. After the previous analyses of the 'sparkles' were published (Mowla et al. 2022; Claeyssens et al. 2023; Adamo et al. 2023), STARRED (Millon et al. 2024; Michalewicz et al. 2023), a sophisticated photometry pipeline, specially developed to handle this challenge, became available. Here, we apply this new methodology to the Sparkler and illustrate how these objects can be used as cosmic clocks.

2. Data and methodology

The data used in this work are the reduced JWST NIRCam images of SMACS J0723.3-7327 in the F090W, F150W, F200W, F277W, F356W and F444W bands provided by Mowla et al. (2022) (M22, hereafter). These images have been reduced through a combination of a modified *JWST* pipeline and the `Grizly` software (Brammer & Matharu 2021) and have a pixel scale of 0.04″ per pixel. Full details on the image processing are provided in Noirot et al. (2023).

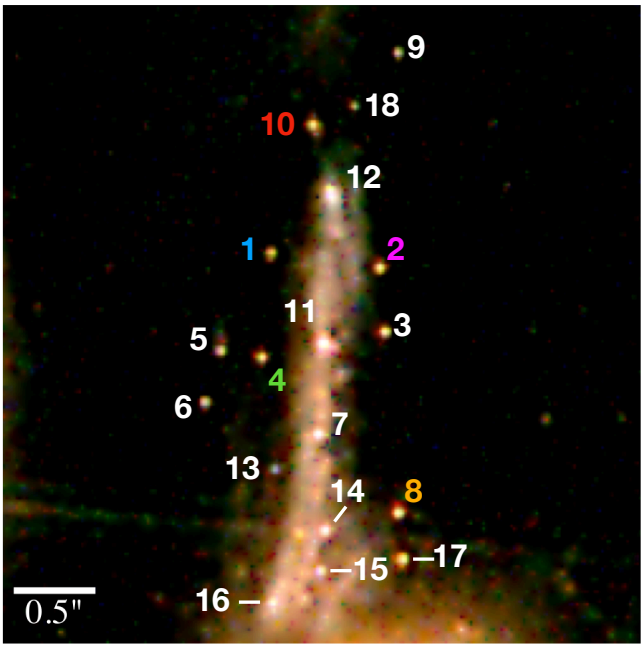

Fig. 1. Colour composite region of 4″on-a-side around the Sparkler. The figure is adapted from Millon et al. (2024) and indicates the labelling of the different objects. The colour code corresponds to the one in Fig. 3. The PSF in this STARRED-deconvolved image is a circular Gaussian with a FWHM of 0.04″.

Previous studies on the Sparkler system have relied on different photometric methods to derive the properties of its compact sources. M22 used fixed-aperture photometry, while Claeyssens et al. (2023) employed PSF-fitting techniques following the approach of Messa et al. (2019, 2022). Adamo et al. (2023) further reanalysed both photometric datasets using a different SED-fitting code. In this work, we present a completely new photometric analysis of the Sparkler, based on a deconvolution pipeline specifically developed to disentangle point-like sources from the surrounding extended emission.

2.1. STARRED photometry

STARRED (Millon et al. 2024; Michalewicz et al. 2023) performs deconvolution photometry, making it uniquely well suited to isolate the emission from the sparkles from the lensed arc of the host galaxy. In particular, the STARRED algorithm avoids producing Gibbs oscillations around point sources (Magain et al. 1998) and allows the shape of the PSF in the deconvolved image – also known as the target PSF – to be chosen.

Because Gaussians do not contain high spatial frequencies, the target PSF is chosen to be a (circular) Gaussian, as opposed to a Dirac function as implemented in all other algorithms. The deconvolved images are also decomposed into two channels, one containing all the analytical Gaussian point sources, and one containing a pixelated image of anything extended. Wavelet regularisation is applied to the latter to enforce the sparsity of the final deconvolved data.

The output is a list of positions and intensities of all the point sources, along with their error bars, as well as an image of the

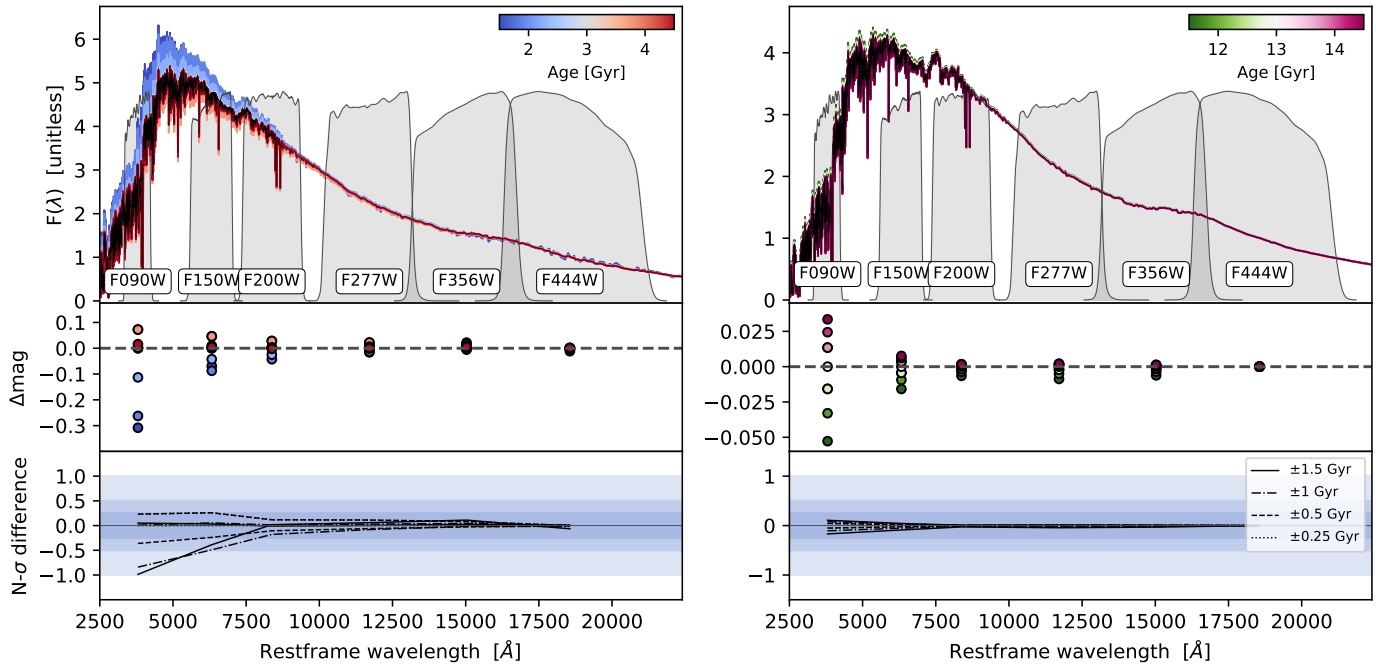

Fig. 2. Sensitivity of the SED of GCs to absolute age, estimated for the six photometric bands considered in this study. The SEDs are shown in the top panels, for a delayed SFH with $\tau = 0.1$ Gyr and Kroupa IMF (Kroupa 2001) (see Sect. 2.2 for more details), along with the filter transmission functions used for studying the Sparkler. The left panels show the typical SED of a young population (age ∼1.5–4.5 Gyr), while the right panels present an older population (age ∼11.5–14.5 Gyr). All SEDs are normalised to the flux in the redder photometric band (the one with the smaller error). The middle panels show the difference in magnitude with respect to a reference age, considering 3 Gyr and 13 Gyr, respectively for the left and right panels. The bottom panels report the significance of the estimated differences normalised by the typical errors in the various bands for the Sparkler's photometry, where the shaded regions show the 0.25, 0.5, and 1σ regions.

extended light in the data, with no need to introduce any analytical representation. The same method can be used to obtain very accurate PSFs, even as complex as the JWST ones, including all Airy rings, spikes, and diffraction artefacts. A recent example of an application of this algorithm consists of light curves of very blended lensed quasar images (see Fig. 2 of Dux et al. 2025).

The photometry and the PSF used in the present work are the same as in Millon et al. (2024), which uses the Sparkler as a test case for the method. STARRED was applied to the JWST data for all six bands available for the Sparkler (see Fig. 1). Note that the spatial resolution achieved on the Sparkler with STARRED is 0.04″ (Fig. 1). This is at least 10 times larger than the physical size of GCs at $z = 1.38$, leaving them indistinguishable from point sources. Indeed, the extended channel of the deconvolved images does not show any trace of residual extended light in any band.

As STARRED also offers the possibility to compute non-analytical and sub-sampled PSFs as well as a wavelet-regularised treatment of the extended arc, we consider only the STARRED photometry below (as listed in Table 3 of Millon et al. 2024). In particular, we analyse all 18 compact objects detected by Millon et al. (2024), including newly identified point sources (IDs 13–18) that are not present in the M22 catalogue (see Fig. 1). The candidate GCs, already identified in M22 owing to the absence of [OIII] λ5007 emission and their urJ colours, are here outlined with Source IDs 1, 2, 4, 8, and 10. Notably, Source IDs 5, 6, 7, 11, and 12 appear extended, with flux residuals observed in the extended channel near these point sources (see Millon et al. 2024, for further discussion). While it is not clear whether these spatial extensions are physically associated with the objects or if they are unrelated, STARRED decontaminates, by construction, the flux of the point-like objects from that of any sources present in the extended channel of the deconvolved image.

Finally, let us note that the magnification by the lensing galaxy cluster is about $\mu = 12$ (Claeyssens et al. 2023, C23 hereafter) across the entire field of view in Fig. 1. This illustrates that the lensing caustic is shallow and that chromatic effects due to lensing are negligible, even in the case where intrinsic colour gradients are present in the lensed sources.

2.2. Determining ages and metallicities

We measured the age, metallicity, and dust reddening of all the sources detected by Millon et al. (2024) using the public code `BAGPIPES` (Carnall et al. 2018). `BAGPIPES` allows us to fit photometry by adopting a parametric Bayesian approach, maximising the posterior probability via the nested sampling algorithm `Multinest` (Buchner 2016). A detailed description of all the code's features is presented in Carnall et al. (2019) and Carnall et al. (2022).

To date, SED fitting on the sparkles has been performed either via a non-parametric approach – as in M22 with `DenseBasis` (Iyer & Gawiser 2017) – or by adopting a star formation history (SFH) with fixed duration, as in C23 (instantaneous, 10 Myr or 100 Myr long) using SSP models (Yggdrasil, Zackrisson et al. 2011), or in Adamo et al. (2023) (single burst) using `MCMAME` (Usher et al. 2019). In all cases, ages could range up to 4.5–5 Gyr at maximum, as this is approximately the expected age of the Universe at $z = 1.38$. Here, we opt for a parametric approach, choosing a functional form for the SFH but allowing the fit to determine the optimal SFH length, along with all the other physical parameters of the population. The other key difference of this study compared to others in the

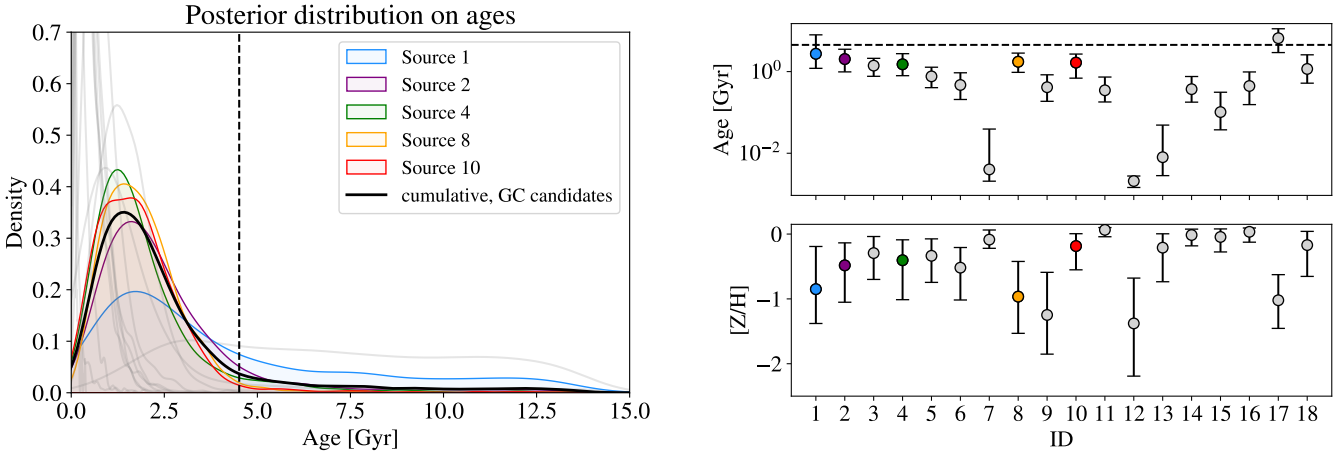

Fig. 3. Left panel: Posterior for the ages of the five GCs in the Sparkler (with the posterior distributions for the other sources marked by thick grey lines). The best fit and 68% credible regions for the ages and metallicities are reported in the right panels. For reference, in both panels, the dashed lines indicate the age of the Universe in a vanilla ΛCDM cosmology.

literature is the removal of the cosmological prior on the age of the stellar population, which allows us to discuss our results within a cosmological context.

The synthetic spectra modelled in `BAGPIPES` to fit the photometry are based on three main components.

The first component involves the use of the 2016 version of the Bruzual & Charlot (2003) stellar population models (hereafter, BC16; see Chevallard & Charlot 2016), which adopt a Kroupa (2001) initial mass function (IMF).

The second component is the assumed SFH of the stellar population, which follows a delayed exponentially declining law, $\propto (t - T_0) \exp^{-(t-T_0)/\tau}$. In this model, T_0 represents the age of the Universe at the onset of star formation, while τ sets the width of the SFH. We adopted a uniform prior for τ, ranging from 0 to 1 Gyr. In this work, a key modification to `BAGPIPES`, already tested and validated in Jiao et al. (2023) and Tomasetti et al. (2023), was applied to allow T_0, and consequently the age of the stellar population, to span the full range of 0–15 Gyr independently of redshift, thereby removing the effects of cosmological assumptions from the age priors.

The third component is dust absorption, modelled with a Calzetti et al. (2000) law to account for the potential presence of dust in the system. A uniform prior is adopted on the parameter A_V in the range 0–4 mag.

In total, we varied six parameters: 1) the age of the oldest stellar population, 2) the SFH width (τ), 3) overall metallicity $[\mathrm{Z/H}] = \log\left(\frac{Z}{Z_\odot}\right)$, 4) dust attenuation ($A_V$), 5) velocity dispersion (σ_v), and 6) stellar mass. Stellar mass and velocity dispersion are effectively nuisance parameters that have no effect on the other parameters; they are therefore not reported. Stellar mass, in particular, acts as a normalisation factor for the SED, but does not affect its shape, which is primarily determined by age, metallicity, and dust attenuation.

Before fitting, we corrected the flux in each filter to account for the Milky Way's foreground extinction, listed in Table 1 of C23.

It is worth observing here that in the age range typical of objects at z ∼ 1.4 population synthesis models can effectively distinguish between younger and intermediate-age populations, which feature intermediate-mass stars with unique photospheric properties. Notably, it is not just the main-sequence turn-off, but also the entire sub-giant branch that is sensitive to age. On the other hand, age determination becomes increasingly challenging for older populations reaching 12 Gyr or more. This is illustrated in Fig. 2, which shows the sensitivity of a GC spectrum to changes in age by comparing two different populations: a younger (∼3 Gyr) and an older one (∼13 Gyr). All the spectra are normalised to the Sparkler band with the smallest photometric error (F444W). It is evident how the younger populations can constrain a difference in ages of ±0.5–1.5 Gyr with a considerably higher significance than older populations.

3. Results

Figure 3 summarises our main results. For all 18 sources, we show the posterior distribution of the ages on the left panel, and on the right panels the central value and the 68.4% confidence interval for the age and metallicity. The GC candidates are highlighted in bright colours. Remarkably, we find that the choice of the upper limit on the prior age does not affect in any significant way the 1– and 2–σ confidence intervals. Despite adopting a very wide prior for the ages (uniform between 0 and 15 Gyr), all the recovered ages are compatible with the ΛCDM model's predictions. For all the parameters except τ, the posteriors are not prior dominated (see the appendix for more details).

The average age of the GC candidates is 1.9 ± 0.4 Gyr, where the error represents the standard deviation. We stress that this is the first time ages for the Sparkler's GC candidates have been derived without imposing a cosmological prior, thereby allowing for their use in a cosmological context. For reference, the flat ΛCDM Planck18-model inferred age of the Universe at redshift z = 1.378 is ∼4.5 Gyr.

For comparison, M22, adopting a non-parametric SED-fitting analysis on fixed-aperture photometry, finds ages for these candidate GCs of approximately 3.9–4.1 Gyr, ∼2 Gyr older than the results found here, and converging at the edge of their adopted cosmological prior. After deriving the SEDs with a Gaussian fitting approach and performing SED-fitting analysis based on SSP models, C23, by contrast, indicates that while two of the five GC candidates have ages of 4 Gyr, aligning with M22's results, the other three show ages around 1 Gyr, compatible with our results. Adamo et al. (2023) reanalysed the photometry for the GC candidates, independently published by M22 and C23, using the `MCMAME` code (Usher et al. 2024) to refine the physical properties of the star clusters. They measure

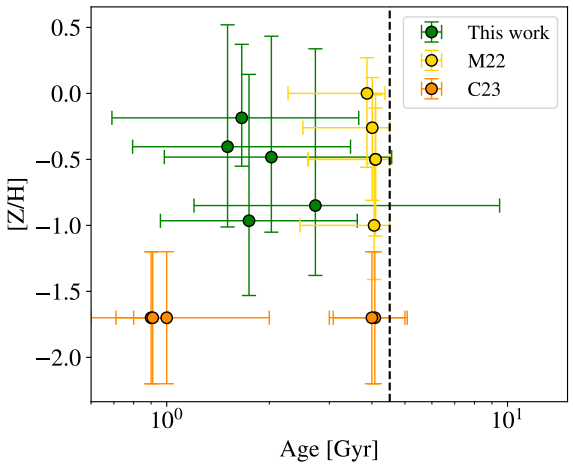

Fig. 4. Overall metallicity vs age for the five GC candidates. The results from this work are shown in green, those from M22 in yellow, and those from C23 in orange. The dashed line indicates the age of the Universe in vanilla ΛCDM.

ages and metallicities that are qualitatively consistent with those found by C23, but since the ages did not converge, they conclude that these GCs are definitively older than 1 Gyr and could be as old as the Universe.

When comparing our results with those from previous studies, it is important to recognise that the reported age estimates – if constrained by a cosmological prior – could be significantly older if that prior were removed.

In terms of metallicity, the GC candidates show a mean [Z/H] = −0.6 ± 0.3. Our results are consistent with those measured in M22 within the errors, although we find them generally lower by ∼ −0.13 dex. C23, by contrast, finds the lowest χ^2 with the SSP set at [Z/H] = −1.7, which is ∼1.1 dex more metal-poor than our results. In their reanalysis of M22 and C23 photometries, Adamo et al. (2023) find on average [Z/H] ∼ −1.7 and [Z/H] ∼ −1.5 respectively, both aligning with C23 estimates. The only exception is source 10, which, when analysed with C23 photometry, yields [Z/H] ∼ −0.2, a value compatible with our findings.

Although beyond the scope of the present paper, the measured ages and metallicities provided here enable the derivation of an age-metallicity relation for the stellar clusters in the Sparkler, making them of broad interest for studies on galaxy formation and chemical enrichment (Forbes & Romanowsky 2023). In Fig. 4 the distribution in the age – metallicity plane for the GC candidates obtained in this work is shown in comparison with the results presented in M22 and C23.

The derived dust reddening is fairly low for the GC candidates, with A_V = 0.3 ± 0.1 mag on average. Non-isolated sources, instead, often show reddening values above 0.5 mag (e.g. sources 7, 11, 12, 16, and 17). To assess how the inclusion of dust reddening impacts the age and metallicity of the GC candidates, we also performed the analysis excluding it from the modelling. On average, we find an increment of ∼1.1 Gyr in age and ∼0.13 dex in metallicity.
The measured ages, metallicities, dust reddening, and SFH width (τ) for the candidate GCs are reported in Table 1.

Table 1. Results of the SED fitting for the five candidate GCs.

ID	Age [Gyr]	[Z/H]	$A_{V,dust}$ [mag]	τ [Gyr]
PRIOR	U(0,15)	U(−4,0.1)	U(0,4)	U(0,1)
1	$2.73^{+5.22}_{-1.53}$	$-0.85^{+0.66}_{-0.53}$	$0.22^{+0.40}_{-0.16}$	$0.61^{+0.24}_{-0.37}$
2	$2.03^{+1.50}_{-1.04}$	$-0.48^{+0.35}_{-0.57}$	$0.27^{+0.38}_{-0.18}$	$0.66^{+0.22}_{-0.34}$
4	$1.51^{+1.24}_{-0.71}$	$-0.40^{+0.31}_{-0.61}$	$0.30^{+0.34}_{-0.21}$	$0.64^{+0.24}_{-0.32}$
8	$1.74^{+1.09}_{-0.78}$	$-0.96^{+0.54}_{-0.57}$	$0.26^{+0.31}_{-0.19}$	$0.68^{+0.21}_{-0.32}$
10	$1.66^{+1.03}_{-0.97}$	$-0.18^{+0.19}_{-0.36}$	$0.46^{+0.48}_{-0.34}$	$0.64^{+0.25}_{-0.24}$

Notes. The adopted uniform priors are indicated as U(x,y), where x and y are the lower and upper limits, respectively. The median value and 68.4% confidence interval for age, metallicity, dust reddening, and τ parameter are reported for each source.

4. Conclusions and future prospects

Cosmic clocks (Jimenez & Loeb 2002) provide a strictly cosmology-independent constraint on the expansion history of the Universe. While cosmic clocks at $z > 1$ were so far exclusively passively evolving galaxies, we explored the possibility of obtaining absolute ages for strongly lensed and magnified GCs at redshifts beyond zero in the lensed Sparkler system, using their integrated six-band photometry from space. The adopted wavelet-based deconvolution-photometry algorithm (STARRED) is uniquely suited to isolate the emission from point-like sources from the complex morphology of the lensed arc of the host galaxy.

For all the lensed Sparkler objects, using a fully Bayesian pipeline, we estimated key parameters, such as age, metallicity, and dust attenuation. Very broad priors (especially on the age) were adopted so as not to introduce cosmological biases. The simultaneous fit of the physical parameters of the GCs and the broad priors adopted, combined with high-quality deconvolution photometry, are key novel aspects of this work.

The GC candidates are point-like and older compared to the other sources. Our main result is that the mean age of the five GC candidates is 1.9 ± 0.4 Gyr. This is fully consistent with the ΛCDM Planck18-model prediction for the age of the Universe at redshift z = 1.38, and is even 2.6 Gyr younger. This is also interesting from the point of view of GC formation, considering that the ages of local GCs are typically comparable to the age of the Universe itself. The difference observed in the Sparkler's candidate GCs may be explained by their higher metallicity, as they lie at the metal-rich end of the distribution ([Z/H] > −1). In the local Universe, GCs in this metallicity range generally exhibit younger ages, typically between 10.5 and 11.5 Gyr (see e.g. VandenBerg et al. 2013; Massari et al. 2019). Adopting the same cosmological model used throughout this work, this corresponds to a delay of approximately 2.5–3.5 Gyr relative to the age of the Universe at z = 0. This is fully consistent with the age difference we find at z = 1.38. The fact that lensed GCs are located towards the more metal-rich end of the GC distribution might be due to a simple selection effect: redder GCs are visible in the IR bands, while metal-poor, bluer GCs may not be.

Our main result, together with the fact that the ages of GCs at z ∼ 1.4 can be measured convincingly, opens up the possibility of using GCs at high-z as cosmic clocks to constrain the cosmological model, should more Sparkler-like magnified GCs be observed at different redshifts. Interestingly, the uncertainty in the age determination for these GCs today is comparable to that of the first passively evolving galaxies whose ages were obtained at a similar redshift (z = 1.5) in the mid-90s (Dunlop et al. 1996). New JWST/NIRSpec (IFU) spectroscopic observations of the Sparkler have been acquired (Cycle 2 GO#2969; PI

Mowla). These spectra, to which we do not have access at the time of this study, will represent a strong blind test and validation of our methodology, which is based solely on photometry. As photometry is feasible with JWST over large fields of view, these five GC candidates likely represent only a small fraction of a much larger population of GCs available for cosmic clock studies. The JWST multi-band imaging of galaxy clusters shows a plethora not only of lensed GCs but also of GCs in the member galaxies of the clusters themselves, potentially providing GC samples at redshifts typical for galaxy clusters ($0.1 < z < 0.8$) and for lensed sources well beyond $z = 1$. Finally, Euclid images – such as those of the Perseus cluster taken as part of the Early Release Observations data – also display numerous (non-lensed) GCs around the very low redshift cluster galaxies (Cuillandre et al. 2025).

A systematic multi-band photometric campaign of GCs in and behind galaxy clusters, based on Euclid and JWST, can enable the measurement of ages for a sizeable population of GCs spanning a broad range of redshifts, which can then be used as cosmic clocks.

Acknowledgements. We thank the anonymous referee for the valuable feedback, which helped us improve the robustness of our findings. E.T. acknowledges the support from COST Action CA21136 – "Addressing observational tensions in cosmology with systematics and fundamental physics (CosmoVerse)", supported by COST (European Cooperation in Science and Technology). Funding for the work of R.J. and L.V. was partially provided by project PID2022-141125NB-I00, and the "Center of Excellence Maria de Maeztu 2020-2023" award to the ICCUB (CEX2019- 000918-M) funded by MCIN/AEI/10.13039/501100011033. M.Mo. acknowledges support from MIUR, PRIN 2022 (grant 2022NY2ZRS 001). M.Mo. and A.C. acknowledge support from the grant ASI n. 2024-10-HH.0 "Attività scientifiche per la missione Euclid – fase E". M.Mi. acknowledges support by the SNSF (Swiss National Science Foundation) through mobility grant P500PT_203114 and return CH grant P5R5PT_225598.

References

Adamo, A., Usher, C., Pfeffer, J., & Claeyssens, A. 2023, MNRAS, 525, L6
Bastian, N., & Lardo, C. 2018, ARA&A, 56, 83
Baumgardt, H., Sollima, A., & Hilker, M. 2020, PASA, 37, e046
Borghi, N., Moresco, M., & Cimatti, A. 2022, ApJ, 928, L4
Brammer, G., & Matharu, J. 2021, https://doi.org/10.5281/zenodo.5012699
Bruzual, G., & Charlot, S. 2003, MNRAS, 344, 1000
Buchner, J. 2016, Stat. Comput., 26, 383
Cabrera-Ziri, I., & Conroy, C. 2022, MNRAS, 511, 341
Calzetti, D., Armus, L., Bohlin, R. C., et al. 2000, ApJ, 533, 682
Caminha, G. B., Suyu, S. H., Mercurio, A., et al. 2022, A&A, 666, L9
Carnall, A. C., McLure, R. J., Dunlop, J. S., & Davé, R. 2018, MNRAS, 480, 4379
Carnall, A. C., McLure, R. J., Dunlop, J. S., et al. 2019, MNRAS, 490, 417
Carnall, A. C., McLure, R. J., Dunlop, J. S., et al. 2022, ApJ, 929, 131
Cezario, E., Coelho, P. R. T., Alves-Brito, A., Forbes, D. A., & Brodie, J. P. 2013, A&A, 549, A60
Chevallard, J., & Charlot, S. 2016, MNRAS, 462, 1415
Cimatti, A., & Moresco, M. 2023, ApJ, 953, 149
Claeyssens, A., Adamo, A., Richard, J., et al. 2023, MNRAS, 520, 2180
Cuillandre, J. C., Bolzonella, M., Boselli, A., et al. 2025, A&A, 697, A11
Dunlop, J., Peacock, J., Spinrad, H., et al. 1996, Nature, 381, 581
Dux, F., Millon, M., Lemon, C., et al. 2025, A&A, 694, A300
Forbes, D. A., & Romanowsky, A. J. 2023, MNRAS, 520, L58
Gallart, C., Zoccali, M., & Aparicio, A. 2005, ARA&A, 43, 387
Gonçalves, G., Coelho, P., Schiavon, R., & Usher, C. 2020, MNRAS, 499, 2327
Gratton, R., Bragaglia, A., Carretta, E., et al. 2019, A&A Rev., 27, 8
Iyer, K., & Gawiser, E. 2017, ApJ, 838, 127
Jiao, K., Borghi, N., Moresco, M., & Zhang, T.-J. 2023, ApJS, 265, 48
Jimenez, R., & Loeb, A. 2002, ApJ, 573, 37
Jimenez, R., Cimatti, A., Verde, L., Moresco, M., & Wandelt, B. 2019, J. Cosmol. Astropart. Phys., 2019, 043
Jimenez, R., Moresco, M., Verde, L., & Wandelt, B. D. 2023, J. Cosmology Astropart. Phys., 2023, 047
Koleva, M., Prugniel, P., Ocvirk, P., Le Borgne, D., & Soubiran, C. 2008, MNRAS, 385, 1998
Kroupa, P. 2001, MNRAS, 322, 231
Lotz, J. M., Koekemoer, A., Coe, D., et al. 2017, ApJ, 837, 97
Magain, P., Courbin, F., & Sohy, S. 1998, ApJ, 494, 472
Mahler, G., Jauzac, M., Richard, J., et al. 2023, ApJ, 945, 49
Massari, D., Koppelman, H. H., & Helmi, A. 2019, A&A, 630, L4
Messa, M., Adamo, A., Östlin, G., et al. 2019, MNRAS, 487, 4238
Messa, M., Dessauges-Zavadsky, M., Richard, J., et al. 2022, MNRAS, 516, 2420
Michalewicz, K., Millon, M., Dux, F., & Courbin, F. 2023, J. Open Source Softw., 8, 5340
Millon, M., Michalewicz, K., Dux, F., Courbin, F., & Marshall, P. J. 2024, AJ, 168, 55
Milone, A. P., & Marino, A. F. 2022, Universe, 8, 359
Moresco, M. 2015, MNRAS, 450, L16
Moresco, M., Cimatti, A., Jimenez, R., et al. 2012, J. Cosmology Astropart. Phys., 2012, 006
Moresco, M., Pozzetti, L., Cimatti, A., et al. 2016, J. Cosmology Astropart. Phys., 2016, 014
Moresco, M., Amati, L., Amendola, L., et al. 2022, Liv. Rev. Relativ., 25, 6
Mowla, L., Iyer, K. G., Desprez, G., et al. 2022, ApJ, 937, L35
Noirot, G., Desprez, G., Asada, Y., et al. 2023, MNRAS, 525, 1867
Pontoppidan, K. M., Barrientes, J., Blome, C., et al. 2022, ApJ, 936, L14
Ratsimbazafy, A. L., Loubser, S. I., Crawford, S. M., et al. 2017, MNRAS, 467, 3239
Tomasetti, E., Moresco, M., Borghi, N., et al. 2023, A&A, 679, A96
Tomasetti, E., Moresco, M., Lardo, C., Cimatti, A., & Jimenez, R. 2025, A&A, 696, A98
Usher, C., Brodie, J. P., Forbes, D. A., et al. 2019, MNRAS, 490, 491
Usher, C., Caldwell, N., & Cabrera-Ziri, I. 2024, MNRAS, 528, 6010
Valcin, D., Bernal, J. L., Jimenez, R., Verde, L., & Wandelt, B. D. 2020, J. Cosmology Astropart. Phys., 2020, 002
VandenBerg, D. A., Brogaard, K., Leaman, R., & Casagrande, L. 2013, ApJ, 775, 134
Zackrisson, E., Rydberg, C.-E., Schaerer, D., Östlin, G., & Tuli, M. 2011, ApJ, 740, 13

Appendix A: SED fitting results

To better illustrate the full parameter posteriors, we show in Fig. A.1 2D contours for different parameter pairs. Note that the age is always very well constrained and that in general, all contours do close. The insets show the derived spectrum from BAGPIPES using the six photometric bands used in this study (blue points for the data and yellow points for the model).

All the best-fit spectra reproduce very well the observed photometry, except for the filter F150W, where the modelled flux is systematically underestimated. Thus, we tried redoing the analysis masking that photometric point, finding that ages are very stable, just ~0.2 Gyr younger on average, and metallicities ~0.2 higher.

Fig. A.1: Joint posteriors for the four parameters studied for the Sparkler. The blue points indicate the data, while the orange points represent the best fit and the corresponding spectrum from BAGPIPES.